ADVANCED FUNCTIONAL MATERIALS
www.afm-journal.de

www.MaterialsViews.com

Multi-Charged Conjugated Polyelectrolytes as a Versatile Work Function Modifier for Organic Electronic Devices

Byoung Hoon Lee, In Hwan Jung, Han Young Woo, Hong-Ku Shim, Geunjin Kim, and Kwanghee Lee**

Despite the excellent work function adjustability of conjugated polyelectrolytes (CPEs), which induce a vacuum level shift via the formation of permanent dipoles at the CPE/metal electrode interface, the exact mechanism of electron injection through the CPE electron transport layer (ETL) remains unclear. In particular, understanding the ionic motion within the CPE ETLs when overcoming the sizable injection barrier is a significant challenge. Because the ionic functionality of CPEs is a key component for such functions, a rigorous analysis using highly controlled ion density (ID) in CPEs is crucial for understanding the underlying mechanism. Here, by introducing a new series of CPEs with various numbers of ionic functionalities, energy level tuning at such an interface can be determined directly by adjusting the ID in the CPEs. More importantly, these series CPEs indicate that two different mechanisms must be invoked according to the CPE thickness. The formation of permanent interfacial dipoles is critical with respect to electron injection through CPE ETL (≤ 10 nm, quantum mechanical tunneling limit), whereas electron injection through thick CPE ETL (20–30 nm) is dominated by the reorientation of the ionic side chains under a given electric field.

1. Introduction

Conjugated polyelectrolytes (CPEs) are conjugated polymers with pendant groups bearing ionic functionalities in cationic, anionic, or zwitterionic form (**Figure 1**a).[1–9] Because of the ionic nature of the side chain, CPEs are soluble in typical polar solvents (e.g., methanol, water, etc.) and enable multilayer stacking in the fabrication of organic devices without intermixing with a pre-coated non-polar conjugated polymer layer.[1,3] The solution-processed fabrication of the CPE layer underneath (or on top of) the active layer, together with its ionic functionality, makes CPEs promising interfacial layer materials in organic electronic devices.[1,3,10–16] By placing the CPEs between the active layer and electrode (both cathode and anode), the work function (WF) of the adjacent metal electrode can be modified; therefore, we can rearrange the energy levels at the metal/semiconductor interface.[1,10,16–20] The WF adjustability of the CPEs results in their widespread application in organic electronic devices adapting the typical thin-film device structure of a metal/semiconductor/metal configuration, in which energy level matching between the metal electrode and semiconducting layer is crucial for achieving a high-performance device.[21–23]

Dr. B. H. Lee, G. Kim, Prof. K. Lee
School of Materials Science and Engineering
Heeger Center for Advanced Materials
Research Institute for Solar and Sustainable Energies
Gwangju Institute of Science and Technology
Gwangju, 500–712, Korea
E-mail: klee@gist.ac.kr
Dr. I. H. Jung, Prof. H.-K. Shim
Department of Chemistry
Korea Advanced Institute of Science and Technology
Daejeon, 305–701, Korea
Prof. H. Y. Woo
Department of Cogno-Mechatronics Engineering (WCU)
Pusan National University
Miryang, 627–706, Korea
E-mail: hywoo@pusan.ac.kr

DOI: 10.1002/adfm.201301810

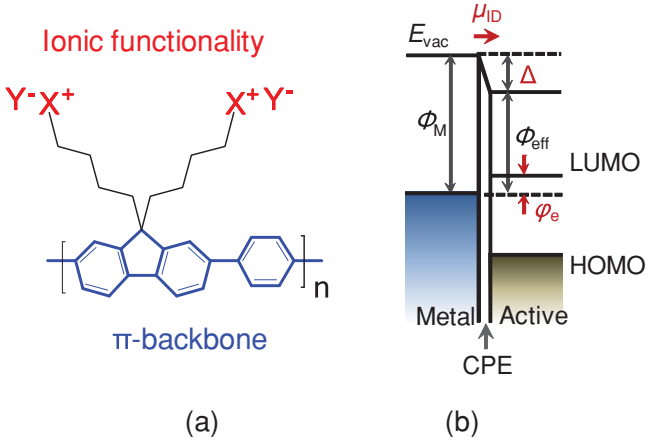

Figure 1. a) Representative molecular structure of cationic CPE consisting of PFP π-conjugated backbone (blue line) and ionic functionalities (red characters). X^+ and Y^- characters represent cationic functionalities that are covalently bonded to alkyl side chains and electrostatically bonded counter ions, respectively. b) Schematic energy level diagram of the metal/CPE/active layers in conventional organic electronic devices. The introduction of a thin CPE layer results in a vacuum level (E_{vac}) shift at the metal/active interface by the formation of interfacial dipoles (μ_{ID}) pointing toward the active layer and decreases the effective WF (Φ_{eff}), which is proportional to the magnitude (Δ) of the generated interfacial dipoles. This process leads to a decreased electron injection barrier (Ψ_e).

Despite the potential of CPEs as an efficient interlayer in many organic electronic applications, including a WF modifier and/or an energy barrier-adjusting electron transport layer (ETL), the manner in which their ionic functionality groups evolve to establish such functions inside the CPE layers is not yet fully understood.[24–28] For example, one of the well-known mechanisms is the interfacial dipole model.[10,16,18,29] When a thin CPE layer with a thickness of a few nanometers (typically <10 nm) is deposited on top of a metal surface, the ionic functionalities somehow lead to the formation of permanent dipoles and induce a shift in the vacuum level at the metal/CPE interface,[18,19] as described in Figure 1b. This vacuum level shift results in a change in the effective WF of the CPE-covered metal electrode. In such a case, neither the manner in which the permanent dipoles are generated from the ionic functionalities of the CPEs nor the factors that determine the magnitude of the interfacial dipoles have been thoroughly explained.

Although we can simply attribute the WF tuning mechanism to the permanent dipole formation for the cases of thin CPE films (typically <10 nm), the cases using thick CPE films (>10 nm) are more complicated in terms of the underlying mechanism. One of the well-known applications of thick CPE films is the application of CPEs to polymer light-emitting diodes (PLEDs). When a CPE is employed as an energy barrier-adjusting ETL with a typical thickness of approximately 20–30 nm in PLEDs using an Al electrode, the devices outperform devices using Ca electrodes without CPEs. However, the simple interfacial dipole model fails to explain the detailed mechanism regarding how the CPE layer facilitates the injection of electrons despite the significant energy barrier between the Al electrode ($WF_{Al} \approx 4.3$ eV) and the lowest unoccupied molecular orbital (LUMO) of the luminescent polymers (typically 2–3 eV), resulting in superior performance in comparison to the PLEDs using a Ca electrode ($WF_{Ca} \approx 2.9$ eV). Although previous results using various CPEs—bearing different counter ion,[1,12,17] different polarity of ionic functionality,[30] or different backbone[3]—have suggested WF tuning mechanisms in PLEDs, there was no systematic study using series CPEs with different ion density (ID).

Because the ionic functionality of CPEs is a key component for energy level tuning at the CPE/metal interface,[12,17–19,25,26,30] a quantitative analysis with increasing ID in the CPEs is expected to aid in the understanding of the underlying mechanisms of the CPE ETLs. In this work, by introducing a new series of cationic CPEs with various numbers of ionic functionalities, we investigated the effect of ID on the energy level tuning process at the CPE/metal interface in the organic electronic devices, which has not been established thus far. By rigorously investigating the electron injection/extraction properties in the PLEDs and polymer solar cells (PSCs) with the series CPE ETLs, we found that two different mechanisms must be invoked to explain the electron injection process in the CPE ETLs. The thickness-dependent electron injection/extraction characteristics at the interface between the series CPEs and metal electrodes provide a comprehensive perspective of the ionic motion inside the CPE layers for enhancing the efficiency of organic electronic devices.

2. Results and Discussion

2.1. CPEs with Various Numbers of Cationic Charges

The molecular structures of the CPE series samples (P1 – P5) used in this study are presented in **Figure 2**a. While all of the samples have an identical poly(fluorene-*co*-phenylene) PFP π-conjugated backbone, each sample exhibits a different number of cationic charged quaternary ammonium functionalities (N^+), attached to the alkoxy side chains with bromide counter ions (Br^-). As P1 changes to P5, the ID steadily increases in the repeat unit of PFP, where ID = 2 for P1, 3 for P2, 4 for P3, 5 for P4, and 6 for P5. The enhanced ID of our samples was directly confirmed by comparing the intensity of the alkyl (R-C-N^+) stretching peak relative to the aromatic (C=C) stretching peak in the Fourier transform infrared (FTIR) spectra[31] (see Figure 2b) as well as by integrating the signal intensity for $-CH_2X$ [$X = N^+(CH_3)_3Br^-$] in the proton nuclear magnetic resonance (^{1}H-NMR) spectra (see Supporting Information).

Although the number of ionic functionalities is different for each sample, the electronic structure of the main backbone (i.e., PFP) of the series samples is not influenced by the ionic functionalities. The CPE films exhibit almost identical optical absorption spectra with a peak at wavelength λ of approximately 370 nm, which corresponds to the delocalized π–π^* transition in the PFP backbone. The films also demonstrate photoluminescence at λ_{max} of approximately 420 nm, as shown in Figure 2c. Cyclic voltammetry was used to estimate the frontier molecular orbital energy levels (see Figure S1, Supporting Information). The highest occupied molecular orbital (HOMO) and LUMO levels were estimated to be –5.6 and –2.6 eV, respectively, for each CPE with an optical bandgap of 3 eV ($\lambda_{onset} \approx 420$ nm, see Figure 2c). Moreover, the series CPE samples exhibit similar molecular weights of approximately 10 KDa and an electron mobility μ of approximately 10^{-2} cm^2 V^{-1} s^{-1}, as obtained from the gel permeation chromatography (GPC) and time-of-flight (ToF) measurements, respectively (see Figure S2 and Table S1, Supporting Information). All measurements indicate that we successfully synthesized a series of CPE samples with various numbers of ionic functionalities without disturbing the π-electronic structure of the main backbone. The complete synthetic and characterization details can be found in the Supporting Information.

2.2. Work Function Tuning with CPEs

Ultraviolet photoelectron spectroscopy (UPS) is a powerful tool for estimating the WF change and vacuum level shift (Δ) at the metal/interfacial layer. **Figure 3**a presents the UPS results of the CPE-covered indium-tin-oxide (ITO) electrodes. For the measurements, thin CPE films with a thickness of approximately 2 nm were cast from methanol/isopropanol (2:1 by volume) solutions on top of pre-cleaned ITO/glass substrates. By increasing the ID from two (P1) to six (P5), the secondary cutoff (16–18 eV) of the CPE-covered ITO electrodes successively shifts to higher binding energies, indicating a monotonic

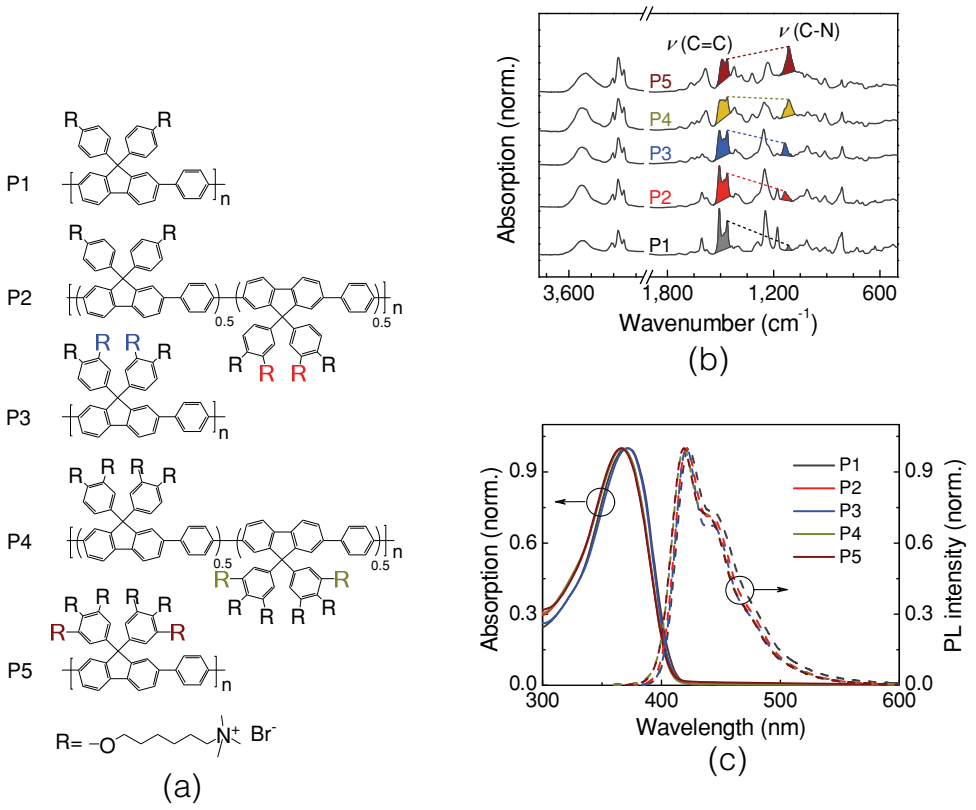

Figure 2. a) Molecular structures of series CPEs with increasing ID per repeating unit from two (P1) to six (P5). The symbol R represents the alkoxy side chain bearing cationic charged quaternary ammonium functionalities (N^+) with bromide counter ions (Br^-). b) FTIR spectra of the series CPE films on the zinc selenide (ZnSe) substrates. c) Ultraviolet-visible absorption (solid lines) and photoluminescence (dashed lines) spectra of the series CPE films on the quartz substrates.

decrease in the effective WF of the ITO electrodes (see Figure 3b). For the P5/ITO electrode, the effective WF is approximately 3.9 eV, which is almost 1 eV lower than that of the bare ITO ($WF_{ITO} \approx 4.9$ eV).

We attribute the gradual WF change to the increased surface coverage of the assembled N^+-Br^- functionalities at the ITO/CPE interface, as illustrated in Figure 3c. Because Br^- ions have a relatively high degree of freedom in methanol solution, they can be preferentially located on the ITO surface during the film formation process due to the enhanced surface tension of the ultraviolet/ozone-treated ITO surface. Subsequently, the N^+ functionalities in the alkoxy side chains are tethered to the Br^--covered ITO surface by electrostatic interactions between N^+ and Br^-, thereby forming permanent dipoles pointing outward from the ITO surface. In this case, the force required to locate the Br^- counter ions on the ITO surface arises from the image charge of the Br^- ions in the ITO substrate, resulting from its high dielectric constant.[27] In fact, this explanation is supported by the recent UPS study[18] that cationic CPEs bearing negatively charged counter ions (Y^-) yield dipoles pointing toward the active layer (which is consistent with our observation), whereas anionic CPEs with positively charged counter ions (Y^+) lead to the formation of dipoles pointing toward the metal surface (the opposite direction in comparison to our case).

Our observation also implies that fine tuning of the effective WF of the metal electrodes is possible by simple solution coating of the CPEs, in which the ID can be adjusted through a 'rational' molecular design. The energy level-matched ITO/CPE electrodes are expected to be more efficient for the charge extraction/injection in organic electronic devices, thereby increasing the device performance.

2.3. Polymer Solar Cells with ITO/CPE Electrodes

To evaluate the influence of the effective WF change (with increasing ID) of the ITO/CPE electrodes on the device performance, we investigated the photovoltaic characteristics of bulk-heterojunction (BHJ) PSCs containing ITO/CPE electrodes with an inverted architecture of ITO/CPE/poly(3-hexylthiophene-2,5-diyl) (P3HT):[6,6]-phenyl C_{61}-butyric acid methyl ester (PCBM)/poly(3,4-ethylenedioxylthiophene):poly (styrenesulfonate) (PEDOT:PSS)/Ag. A schematic device structure and the corresponding energy level diagram are shown in **Figures 4**a and b, respectively. Due to the reduced WF of the ITO/CPE electrodes, the WF difference between the ITO/CPE cathode and the PEDOT:PSS/Ag anode increases, inducing larger internal field within the device that enables the efficient

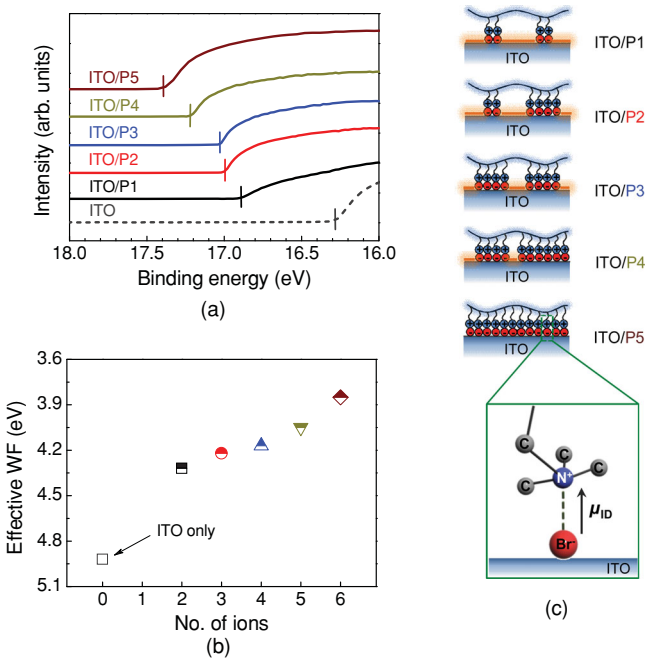

Figure 3. a) Ultraviolet photoelectron spectra of ITO electrodes covered with series CPEs within the range of 16–18 eV (electron cut-off region). b) Changes in the effective WF of the CPE-covered ITO electrodes as a function of ID. c) Schematic illustrations of the proposed configuration of ionic functionalities on the ITO surface with increasing ID (P1→P5) and an enlarged view of the ITO/CPE interface containing the ion-induced μ_{ID} (green box). Orange lines indicate the uncovered region of the ITO surface.

collection of electrons to the ITO/CPE electrodes in a short-circuit condition.

Figure 4c presents the current density-voltage (J–V) characteristics of the devices under simulated AM 1.5G irradiation with an irradiation intensity of 100 mW cm^{-2}, and the device performance parameters are summarized in **Table 1**. The PSC device without CPE shows a rather low power conversion efficiency (PCE) of approximately 1%, with poor device parameters (see Table 1). This lower PCE value originates from two main reasons. 1) Internal electric field (E) of the device (without CPE) in the short circuit condition is not sufficient to sweep out the photo-generated charge carriers due to the relatively small WF difference between the ITO cathode and PEDOT:PSS/Ag anode.[32] 2) Poor electrical contact between the inorganic ITO and the organic photoactive layer in the devices without a CPE layer leads to lower performance of the devices.[33] In contrast, the PSCs using the CPE interfacial layers exhibited enhanced PCEs (2–4%). For PSC fabrication, we used thin CPE films (≈2 nm) as a WF modifier rather than an ETL to simulate the conditions of the UPS experiments, as described above. When increasing the ID of the CPE interfacial layers (from ID = 2 for P1 to ID = 6 for P5), the PCE gradually increased from 2 to 4%. The PCE change (right panel of Figure 4c) is in good agreement with the WF changes of the ITO/CPE electrodes (see Figure 3b), indicating the typical characteristics of a Schottky-Ohmic transition[32,34] at the metal/semiconductor contact, as depicted in Figure 4b. The formation of an Ohmic contact at the ITO/CPE interface leads to reduced sereis resistance of the BHJ solar cells (see inset of right panel of Figure 4c) and significant enhancement of fill factor (FF) of the devices. The device using the P5 interfacial layer with the highest ID yielded a maximum PCE of 4% with a short-circuit current density (J_{sc}) of 9.5 mA cm^{-2}, an open-circuit voltage (V_{oc}) of 0.61 V, and an FF of 70%. Moreover, the P5 device did not exhibit any harmful light-soaking problem,[35–38] which has been an obstacle in realizing high-performance inverted PSCs due to the mismatched energy level at the ITO/active layer interface.[35,38] The series CPEs were also suitable for various active systems comprised of efficient donor material, resulting in a high PCE of 6.2% for an inverted PSC using the P5 interfacial layer (see Figure S3, Supporting Information). Our observation implies that the energy level matching at the CPE/metal interfaces can be accomplished by tailoring the ionic functionalities of the CPEs.

Figure 4d presents the J–V curves of the inverted PSCs, fabricated with P5 in various film thicknesses (δ_{P5} ≈ 2–50 nm). While the data exhibit a maximum PCE of 4% at a δ_{P5} of approximately 2 nm, the PCE value gradually decreases with increasing δ_{P5} up to 32 nm and exhibits almost-failed device features at a δ_{P5} of approximately 50 nm. We attribute this observation to the reduced internal E with increasing δ_{P5} values.[24,39] Additionally, the performances of the PSCs with relatively thick (≥10 nm) CPE interfacial layers were not proportional to

Table 1. Performance parameters of the PSCs and PLEDs used in this study. All parameters were obtained from the best devices except the average PCE and η_{Lmax} values that were obtained from the measurements using ten devices. In the PLED dataset, the values in the parentheses represent the data obtained from the device using the Ca/Al cathode without a CPE EIL, whereas the other devices use an Al cathode with and without CPE EILs.

CPE	PSC					PLED			
	V_{oc} [V]	J_{sc} [mA cm^{-2}]	FF [%]	PCE [%]		J_{max} [mA cm^{-2}]	L_{max} [cd m^{-2}]	η_{Lmax} [cd A^{-1}]	
				Average	Best			Average	Best
- (Ca)	0.37	7.61	37	0.7 ± 0.2	1.0	720 (1270)	120 (10 680)	0.01 ± 0.01 (0.77 ± 0.05)	0.02 (0.83)
P1	0.54	8.98	41	1.9 ± 0.1	2.0	550	660	0.11 ± 0.01	0.12
P2	0.60	9.28	48	2.4 ± 0.1	2.6	630	2,580	0.35 ± 0.05	0.40
P3	0.61	9.37	59	3.1 ± 0.1	3.3	1,120	16,400	1.34 ± 0.09	1.45
P4	0.61	9.45	64	3.6 ± 0.1	3.7	880	5,980	0.62 ± 0.04	0.68
P5	0.61	9.53	70	3.9 ± 0.1	4.0	680	1,280	0.15 ± 0.02	0.18

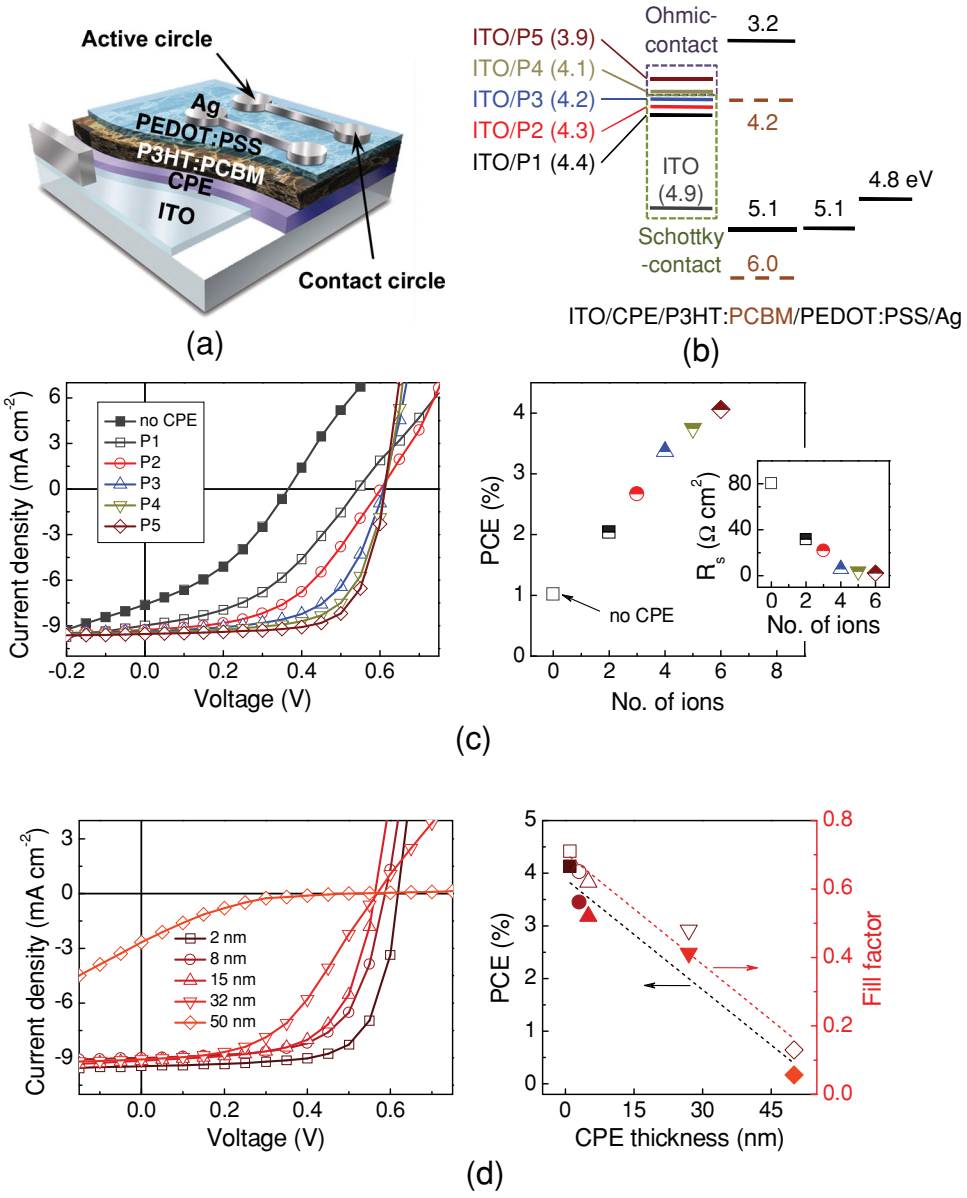

Figure 4. a) Schematic device structure of the inverted PSC used in this study for ITO/CPE/P3HT:PCBM (120 nm)/PEDOT:PSS (30 nm)/Ag. b) Corresponding energy level diagrams of the devices using series CPEs as WF modifiers. c) Left panel: *J–V* characteristics of the inverted PSCs with (open symbols) and without (solid symbol) CPE interfacial layers ($\delta \approx 2$ nm). Right panel: PCE values of the devices as a function of ID. Inset shows the series resistances of the devices extrapolated at the V_{oc}. d) Left panel: *J–V* curves of the inverted PSCs using the P5 interfacial layers with different film thicknesses. Right panel: PCE and FF values of the devices with the P5 interfacial layer as a function of the P5 film thickness.

the ID. Thus, for the thin CPE interfacial layer ($\delta \leq$ quantum mechanical tunneling limit), the permanent interfacial dipole is the dominant mechanism for the WF tuning of the CPE-combined metal electrode. The enhanced electron mobilities of organic field-effect transistors (OFETs) with increasing ID of thin ($\delta \approx 3$–5 nm) CPE electron injection layers (EILs) due to reduced contact resistances at series CPE/Au interfaces support our assertions (see Figures S4 and S5 and Table S2, Supporting Information). However, the devices were reasonably operated until a δ_{P5} of 30 nm because of its high electron mobility, as described in the Supplementary Information. In comparison with the thickness-sensitive non-conjugated polyelectrolyte system,[32] this thickness insensitivity allows CPEs to be promising interfacial materials in less elaborate printing technology, such as that used for flexible electronics.[33,40]

2.4. Polymer Light-Emitting Diodes Using CPE EILs

The charge injection characteristics of the CPEs were investigated by fabricating PLEDs using series CPEs as an EIL with a device architecture of ITO/PEDOT:PSS/poly[2-methoxy-5-(2′-

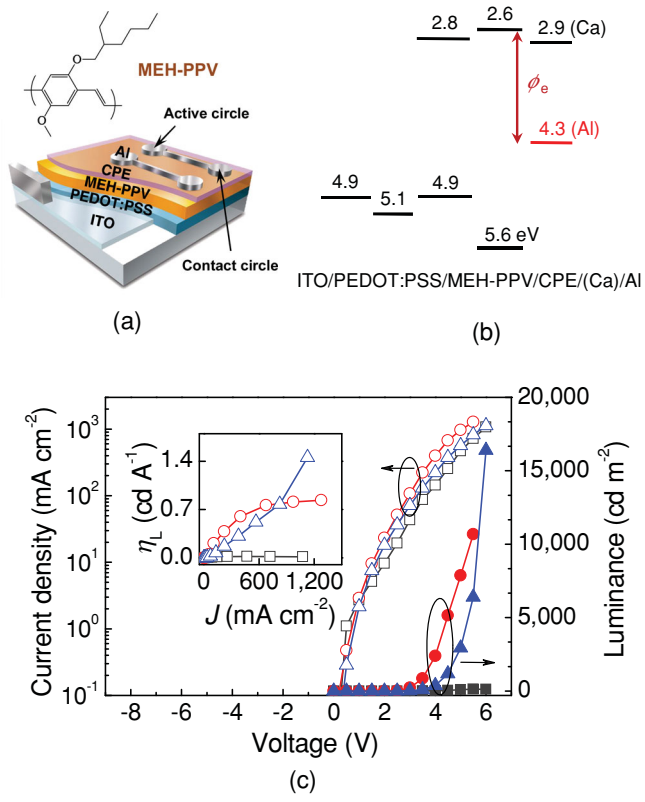

Figure 5. a) Schematic device structure of the PLED used in this study for ITO/PEDOT:PSS (30 nm)/MEH-PPV (80 nm)/CPE/Al and molecular structure of the MEH-PPV. b) Corresponding energy level diagram of the devices with Ca/Al or Al cathode. c) *J*–*V*–*L* characteristics of the PLEDs with Al (grey square), Ca/Al (red circle), or CPE (P3)/Al (blue triangle) cathode. The film thickness of the P3 EIL is approximately 32 nm.

ethylhexyloxy)-*p*-phenylenevinylene] (MEH-PPV)/CPE/Al. The schematic device architecture and molecular structure of the emitting material, MEH-PPV, are shown in **Figure 5**a, together with the corresponding energy level diagram in Figure 5b. The purpose of using CPE-EILs in fabricating high-performance and air-stable PLEDs is clearly demonstrated in Figure 5c, as confirmed by comparing the *J*–*V*-luminance (*L*) characteristics of PLEDs with CPE (P3)/Al, Ca/Al, or Al cathodes. The device with a CPE-EIL exhibited superior performance compared to the device with a Ca/Al cathode despite the high electron injection barrier ($\Psi_e \approx 1.7$ eV) for the CPE/Al cathode (see Figure 5b).

To investigate the ID effect of CPE EILs on the charge injection characteristics in PLEDs, we characterized the device performance of PLEDs using the series CPE EILs, as shown in **Figure 6**a. As the ID increases up to four (P3), the device performance improves gradually. However, when the ID exceeds four, the device performance decreases unexpectedly, as shown in Figure 6b. Consequently, the P3 device yielded the highest values of $L \approx 16\,000$ cd m^{-2}, luminous efficiency (η_L) $\approx$ 1.4 cd A^{-1}, and $J_{max} \approx 1{,}120$ mA cm^{-2} (see Table 1), which are higher than those obtained from the device using a Ca/Al electrode that forms ohmic contact with the LUMO of MEH-PPV (see Figures 5b and c). This ID dependence in the PLED case is inconsistent with the PSC results (Figure 4c) in which the PSC performance increased almost linearly with the ID.

The inconsistence of the CPE application in PLEDs with the PSC case is also observed in the thickness dependence of the CPE EILs, as evident in Figures 6c and d. Whereas the PSCs perform better with decreasing CPE thickness, with a maximum PCE at a δ of approximately 2 nm (Figure 4d), the PLED case is quite the opposite. The PLED performance increases with increasing CPE EIL thickness up to approximately 30 nm. Therefore, we conclude that the underlying mechanism of the EIL using thick CPE layers in PLEDs is not the cases of the PSC and OFET employing a simple interfacial dipole model. Instead, a more complicated model associated with ionic motion should be invoked to explain the CPE EIL mechanism in PLEDs.

2.5. The CPE EIL Model in PLEDs

For a CPE EIL operation mechanism in PLEDs, Hoven and colleagues[12,41] proposed an electron injection process, as illustrated in **Figure 7**a. When a forward bias (V_{app}) is applied to the PLED under the short-circuit condition, the ion pairs (N^+-Br^-) in CPEs are readily polarized. At a given bias, E is redistributed within the CPE layer only due to the hole accumulation at the MEH-PPV/CPE interface because of the easy injection of hole carriers. Subsequently, E is screened via in situ formation of the electric double layer (EDL) after the enforced arrangement of counter ions at both interfaces by an applied E. In fact, E-screening by such an EDL formation is a well-known phenomenon in electrolyte-gated organic field-effect transistors.[9] Therefore, E-screening induces a lowering and thinning of the barriers between the Al electrode and CPE/MEH-PPV layer, thereby allowing for efficient electron injection into the MEH-PPV emitting layer of the PLED device.

2.6. Electric Field Screening by Molecular Reorientation

To induce the E-screening in the proposed mechanism, ionic motion is essential inside the CPE film. However, two detailed mechanisms have been proposed for the ionic motion in CPE films; one is the ion migration model,[1,11,12,24,26,42] and the other is the molecular reorientation model,[8] as shown in Figure **7**b. Under an applied bias, the ions are redistributed by ion migration or molecular reorientation, thereby lowering the electron injection barrier as a result of the in situ formation of a tunnel junction, which is followed by E-screening at the metal/CPE interface. The main difference between the two models is the movement of counter ions against the attractive force between the counter ions (here, Br^-) and ionic functionalities (here, N^+) tethered to the alkyl side chains. In the ion migration model, the counter ions can freely travel to their respective electrodes due to the external E. In contrast, for the molecular reorientation model, the ionic side chains adjacent to the electrode are reoriented under a given E because the counter ions are tightly bound to the ionic functionalities.

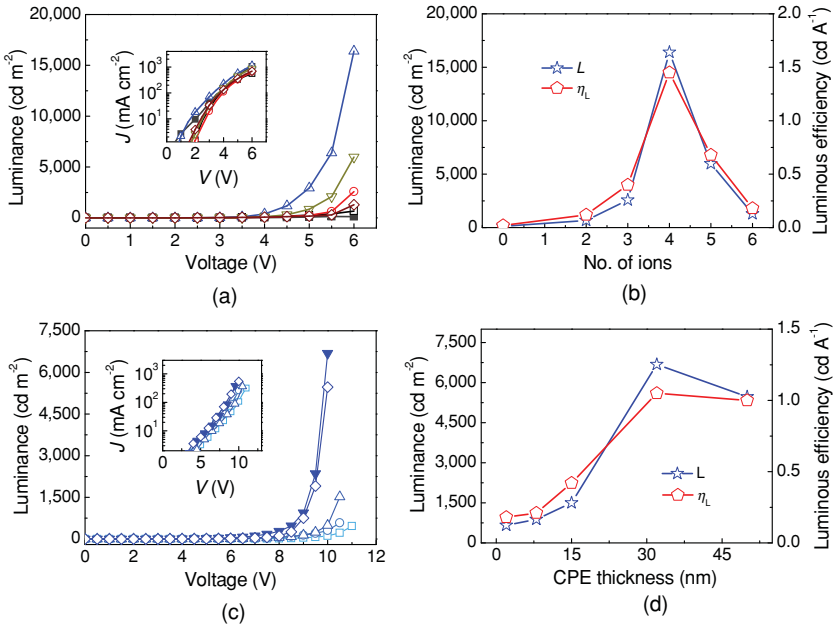

Figure 6. a) *L–V* curves of the PLEDs without (solid symbol) and with (open symbols) CPE EILs ($\delta \approx 32$ nm): P1 (square), P2 (circle), P3 (up triangle), P4 (down triangle), and P5 (diamond). Inset graph shows the *J–V* curves of the same devices. b) Maximum *L* (blue star) and η_L (red pentagon) values as a function of ID of CPE EILs. c) *L–V* curves of the PLEDs using the P3 EILs with various film thicknesses of 2 nm (square), 8 nm (circle), 15 nm (up triangle), 32 nm (down triangle), and 50 nm (diamond). Inset graph shows the *J–V* curves of the same devices. d) Maximum *L* (blue star) and η_L (red pentagon) values as a function of P3 EIL thickness. For the thickness-dependent *J–V–L* measurements, a 150-nm-thick MEH-PPV film was used as an active layer to prevent the breakdown of the PLEDs at high voltages.

By analyzing the device characteristics of PLEDs using the CPE EILs with various IDs and CPE film thicknesses, as shown in Figure 6, we found that our results support the molecular reorientation model rather than the ion migration model in the EDL formation mechanism. This result is particularly true for the ID dependence of the CPE films. If ion migration is more responsible, the larger amount of ions transported by a given E is more effective at screening the external E at the metal/CPE interface, leading to a significant decrease in the electron injection barrier;[12,25,41] thus, enhanced device performance should be obtained from the device by using a CPE EIL with a higher ID (from two to six, P1→P5) due to the enhanced electron injection from the CPE/Al cathode.[21] However, our PLED performance is not proportional to the ID of CPE EILs (see Figures 6a and b). Thus, we speculated that under an applied E, the electron injection through CPE EILs in PLEDs is likely to be associated with the molecular reorientation of ionic side chains near the metal/CPE interface,[8] not long range ion migration. Because tangled PFP wires with a significant amount of ionic side chains results in a more complex structure for the reorientation of the ionic side chains, we attribute the sudden decrease

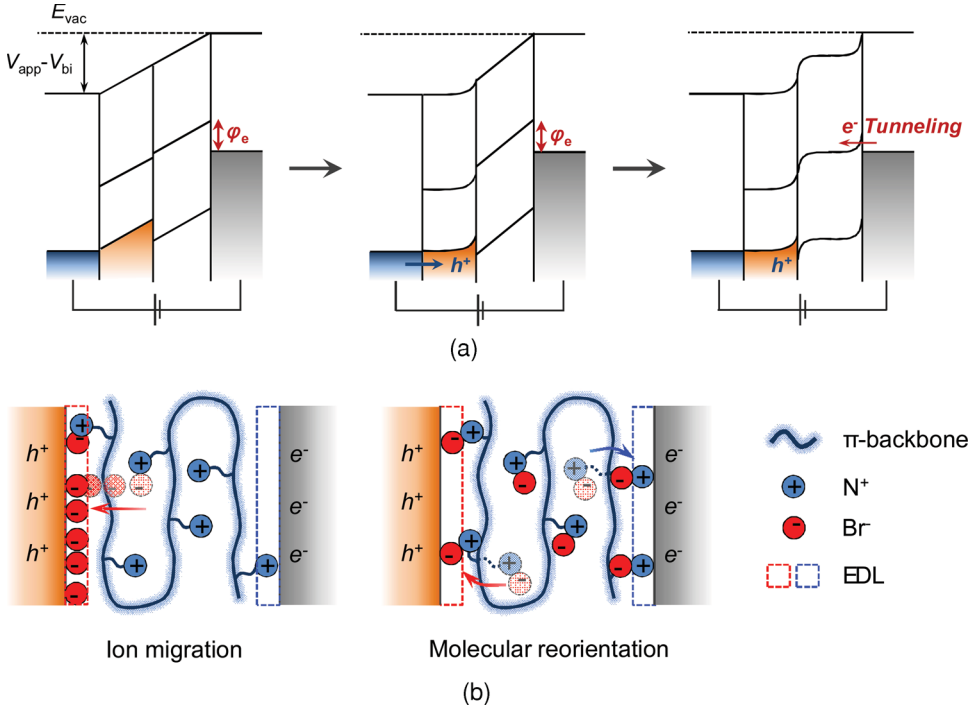

Figure 7. a) Schematic energy level diagrams of an ITO/PEDOT:PSS (blue)/MEH-PPV (orange)/CPE/Al (grey) device under an applied bias (V_{app}) in the electron injection process. V_{bi} represents the built-in-potential of the PLED. b) Schematic illustrations of a partial cross section of the MEH-PPV/CPE/Al layers in the PLED under the V_{app} using the ion migration model (reft) and molecular reorientation model (right).

in the device performance of the PLEDs using the P4 and P5 EILs to kinetically restricted movement of the densely packed ionic side chains, which are tethered to the backbone near the metal surface. Our observation is also consistent with the previously reported results of Garcia and colleagues,[42] who found that the closely packed structures of CPE backbones reduce the device performance and enhance the temporal response time of PLEDs with CPE EILs due to locked ion migration.

3. Conclusions

We have demonstrated electron injection mechanisms into the CPE layers in organic electronic devices by introducing a new series of CPEs with various numbers of ionic functionalities. This is the first report describing systematic design of CPEs with controlled ID by tailoring ionic functionalities in polymeric structures. More interestingly, we found that two different mechanisms should be invoked to understand the electron injection/extraction processes in the devices according to the CPE film thickness; the molecular reorientation model for PLEDs using thick CPE films of approximately 30 nm in thickness and the interfacial dipole model for PSCs adapting thin CPE films of approximately 2 nm in thickness. We expect that more precise control of the molecular structure of the CPE backbone and the ionic functionality will assist in the development of highly efficient organic electronic devices using the CPE functional layers.

4. Experimental Section

The materials and methods for the synthesis and characterization of the monomers and polymers, the cyclic voltammetry plots and ToF spectra of the CPE films, the *J–V* curves and incident photon-to-current efficiency (IPCE) spectra of PSCs, and the transfer curves and device resistance plots of the OFETs can be found in the Supporting Information.

UPS Measurements: The UPS analysis chamber was equipped with a hemispherical electron energy analyzer (AXIS-Nova, SHIMADZU Co. Ltd., Kyoto, Japan), maintained at 1×10^{-9} Torr. The UPS measurements were carried out using the He I ($h\nu$ = 21.2 eV) source. During the UPS measurements, a sample bias of –15 V was used to separate the sample and secondary edge for the analyzer. The samples were kept in a high vacuum chamber overnight to remove the residual solvent before performing the measurements.

PSC Fabrication and Characterization: PSCs with an inverted structure of ITO/CPE/P3HT:PCBM/PEDOT:PSS/Ag were fabricated on ITO electrodes that were wet-cleaned and ultraviolet/ozone-treated. CPE was spin-cast from a methanol/isopropanol (2:1 by volume) solution to form an ultrathin film of approximately 2 nm in thickness. The thickness of the CPE film was determined by the ultraviolet-visible absorption measurements reported previously.[8] The film was dried at 80 °C for 10 min in air and then transferred into a glove box to spin-cast the charge separation layer. The solution, comprised of a blend of P3HT as a donor and PCBM as an acceptor (1:0.8 by weight) in chloroform solvent with a concentration of 10 mg/mL, was then spin-cast on top of the CPE layers. The film was dried at 80 °C for 10 min in the glove box. PEDOT:PSS (Clevios P AI 4083) was then spin-cast from a water/isopropanol (1:7 by volume) solution to form a film measuring 15 nm in thickness. The film was baked at 150 °C for 5 min in the glove box. Then, an Ag (100 nm) electrode was deposited by thermal evaporation in a vacuum of approximately 4×10^{-7} Torr.

The *J–V* characteristics of the devices were measured using a Keithley 238 Source Measure Unit (Keithley Instruments, Inc., Cleveland, OH, USA). The solar cell performance was measured under a calibrated Air Mass 1.5 Global (AM 1.5 G) solar simulator with an irradiation intensity of 100 mW cm^{-2}. An aperture (area ≈ 12.5 mm^2) was used on top of the cell to eliminate the extrinsic effects, such as crosstalk, wave guiding, and shadow effects.

PLED Fabrication and Characterization: PLEDs were fabricated on wet-cleaned ITO electrodes with the structure of ITO/PEDOT:PSS/MEH-PPV/CPE/(Ca)/Al. The ultraviolet/ozone-treated ITO electrode was covered by spin-casting PEDOT:PSS (Clevios P VP AI 4083) with 30 nm in thickness. The substrate was dried at 140 °C for 10 min in air and then transferred to a glove box to spin-cast the emitting layer. The emitting polymer, poly[2-methoxy-5-(2′-ethylhexyloxy)-*p*-phenylenevinylene] (MEH-PPV), was then spin-cast from a 1,2-dichlorobenzene solution (approximately 0.5 wt%) onto the PEDOT:PSS layer. The film was dried at 80 °C for 10 min in the glove box. The MEH-PPV synthesis was performed according to a previous report.[43] The CPE solution diluted in methanol/isopropanol (2:1 by volume) was spin-cast in air on top of the MEH-PPV layer. The samples were baked at 80 °C for 10 min in air and then transferred into a vacuum chamber to deposit the metal electrode. Then, an Al (100 nm) or Ca (20 nm)/Al (100 nm) electrode was deposited by thermal evaporation in a vacuum of approximately 4×10^{-7} Torr.

The device performance was measured inside a glove box at room temperature. The *J–V–L* characteristics were measured using a Keithley 238 Source Measure Unit. The luminance was obtained in the forward-viewing direction using a PR 655 spectrophotometer (Photo Research, Inc., Chatsworth, CA, USA). The active area is 16.2 mm^2.

Supporting Information

Supporting Information is available from the Wiley online Library or from the author.

Acknowledgements

B. H. Lee and I. H. Jung contributed equally to this work. We thank the Heeger Center for Advanced Materials (HCAM) at GIST for their assistance with the measurements. This work was supported by the Core Technology Development Program for Next-Generation Solar Cells of the Research Institute for Solar and Sustainable Energies (RISE) at GIST and the National Research Foundation (NRF) of Korea (2008–0093869, 2008–0062606 (CELA-NCRC), 2012R1A1A2005855, and 2012R1A2A2A06045327).

Received: May 27, 2013
Revised: August 11, 2013
Published online: September 23, 2013

[1] C. V. Hoven, A. Garcia, G. C. Bazan, T.-Q. Nguyen, *Adv. Mater.* **2008**, *20*, 3793.
[2] A. Duarte, K.-Y. Pu, B. Liu, G. C. Bazan, *Chem. Mater.* **2011**, *23*, 501.
[3] F. Huang, H. Wu, Y. Cao, *Chem. Soc. Rev.* **2010**, *39*, 2500.
[4] Y. Liang, Z. Xu, J. Xia, S.-T. Tsai, Y. Wu, G. Li, C. Ray, L. Yu, *Adv. Mater.* **2010**, *22*, E135.
[5] K. Lee, H.-J. Kim, J. Kim, *Adv. Funct. Mater.* **2012**, *22*, 1076.
[6] C. V. Hoven, H. Wang, M. Elbing, L. Garner, D. Winkelhaus, G. C. Bazan, *Nat. Mater.* **2010**, *9*, 249.
[7] D. Wang, X. Gong, P. S. Heeger, F. Rininsland, G. C. Bazan, A. J. Heeger, *Proc. Natl. Acad. Sci. USA* **2002**, *99*, 49.

[8] J. Fang, B. H. Wallikewitz, F. Gao, G. Tu, C. Müller, G. Pace, R. H. Friend, W. T. S. Huck, *J. Am. Chem. Soc.* **2011**, *133*, 683.
[9] U. Scherf, *Angew. Chem. Int. Ed.* **2011**, *50*, 5016.
[10] H. Wu, F. Huang, J. Peng, Y. Cao, *Org. Electron.* **2005**, *6*, 118.
[11] C. Hoven, R. Yang, A. Garcia, A. J. Heeger, T.-Q. Nguyen, G. C. Bazan, *J. Am. Chem. Soc.* **2007**, *129*, 10976.
[12] C. V. Hoven, R. Yang, A. Garcia, V. Crockett, A. J. Heeger, G. C. Bazan, T.-Q. Nguyen, *Proc. Natl. Acad. Sci. USA* **2008**, *105*, 12730.
[13] J. H. Seo, A. Gutacker, Y. Sun, H. Wu, F. Huang, Y. Cao, U. Scherf, A. J. Heeger, G. C. Bazan, *J. Am. Chem. Soc.* **2011**, *133*, 8416.
[14] J. H. Seo, A. Gutacker, B. Walker, S. Cho, A. Garcia, R. Yang, T.-Q. Nguyen, A. J. Heeger, G. C. Bazan, *J. Am. Chem. Soc.* **2009**, *131*, 18220.
[15] C. H. W. Cheng, M. C. Lonergan, *J. Am. Chem. Soc.* **2004**, *126*, 10536.
[16] H. Wu, F. Huang, Y. Mo, W. Yang, D. Wang, J. Peng, Y. Cao, *Adv. Mater.* **2004**, *16*, 1826.
[17] Y. Jin, G. C. Bazan, A. J. Heeger, J. Y. Kim, K. Lee, *Appl. Phys. Lett.* **2008**, *93*, 123304.
[18] J. H. Seo, T.-Q. Nguyen, *J. Am. Chem. Soc.* **2008**, *130*, 10042.
[19] J. H. Seo, R. Yang, J. Z. Brzezinski, B. Walker, G. C. Bazan, T.-Q. Nguyen, *Adv. Mater.* **2009**, *21*, 1006.
[20] S.-H. Oh, S.-I. Na, J. Jo, B. Lim, D. Vak, D.-Y. Kim, *Adv. Funct. Mater.* **2010**, *20*, 1977.
[21] I. D. Parker, *J. Appl. Phys.* **1994**, *75*, 1656.
[22] H. Ishii, K. Sugiyama, E. Ito, K. Seki, *Adv. Mater.* **1999**, *11*, 605.
[23] S. Braun, W. R. Salaneck, M. Fahlman, *Adv. Mater.* **2009**, *21*, 1450.
[24] S.-I. Na, T.-S. Kim, S.-H. Oh, J. Kim, S.-S. Kim, D.-Y. Kim, *Appl. Phys. Lett.* **2010**, *97*, 223305.
[25] J. Park, C. V. Hoven, R. Yang, N. Cho, H. Wu, T.-Q. Nguyen, G. C. Bazan, *J. Mater. Chem.* **2009**, *19*, 211.
[26] R. Yang, A. Garcia, D. Korystov, A. Mikhailovsky, G. C. Bazan, T.-Q. Nguyen, *J. Am. Chem. Soc.* **2006**, *128*, 16532.
[27] J. Park, R. Yang, C. V. Hoven, A. Garcia, D. A. Fischer, T.-Q. Nguyen, G. C. Bazan, D. M. DeLongchamp, *Adv. Mater.* **2008**, *20*, 2491.
[28] R. Yang, H. Wu, Y. Cao, G. C. Bazan, *J. Am. Chem. Soc.* **2006**, *128*, 14422.
[29] C. Duan, L. Wang, K. Zhang, X. Guan, F. Huang, *Adv. Mater.* **2011**, *23*, 1665.
[30] A. Garcia, R. Yang, Y. Jin, B. Walker, T.-Q. Nguyen, *Appl. Phys. Lett.* **2007**, *91*, 153502.
[31] http://www.chemistry.ccsu.edu/glagovich/teaching/316/ir/table.html, accessed August, 2013.
[32] C. J. Brabec, A. Cravino, D. Meissner, N. S. Sariciftci, T. Fromherz, M. T. Rispens, L. Sanchez, J. C. Hummelen, *Adv. Funct. Mater.* **2001**, *11*, 374.
[33] S. K. Hau, H.-L. Yip, O. Acton, N. S. Baek, H. Ma, A. K. Y. Jen, *J. Mater. Chem.* **2008**, *18*, 5113.
[34] Z.-R. Wang, G. Zhang, K.-L. Pey, C.-H. Tung, G.-Q. Lo, *J. Appl. Phys.* **2009**, *105*, 094508.
[35] J. Kim, G. Kim, Y. Choi, J. Lee, S. H. Park, K. Lee, *J. Appl. Phys.* **2012**, *111*, 114511.
[36] J.-C. Wang, C.-Y. Lu, J.-L. Hsu, M.-K. Lee, Y.-R. Hong, T.-P. Perng, S.-F. Horng, H.-F. Meng, *J. Mater. Chem.* **2011**, *21*, 5723.
[37] C. E. Small, S. Chen, J. Subbiah, C. M. Amb, S.-W. Tsang, T.-H. Lai, J. R. Reynolds, F. So, *Nat. Photon.* **2012**, *6*, 115.
[38] R. Steim, S. A. Choulis, P. Schilinsky, C. J. Brabec, *Appl. Phys. Lett.* **2008**, *92*, 093303.
[39] J. S. Kim, J. H. Park, J. H. Lee, J. Jo, D.-Y. Kim, K. Cho, *Appl. Phys. Lett.* **2007**, *91*, 112111.
[40] S. Lee, S. Nam, H. Kim, Y. Kim, *Appl. Phys. Lett.* **2010**, *97*, 103503.
[41] C. V. Hoven, J. Peet, A. Mikhailovsky, T.-Q. Nguyen, *Appl. Phys. Lett.* **2009**, *94*, 033301.
[42] A. Garcia, R. C. Bakus Ii, P. Zalar, C. V. Hoven, J. Z. Brzezinski, T.-Q. Nguyen, *J. Am. Chem. Soc.* **2011**, *133*, 2492.
[43] F. Wudl, G. Srdanov, USA Patent 5189136, **1993**.